

Article

Analysis of the Boss Structure of Type IV Composite Vessel for a High-Pressure Hydrogen Tube Trailer

Zhiwen Meng^{1,2}, Suke Jin^{1,2}, Meng Yu^{1,2}, Abel Mehari³  and Long Jiang^{3,*}

¹ Special Equipment Safety Supervision and Inspection Institute of Jiangsu Province, Nanjing 210036, China; 2111902311@zjut.edu.cn (Z.M.); ym1993@zju.edu.cn (M.Y.)

² Hydrogen Equipment Product Quality Supervision and Inspection Center of Jiangsu Province, Changzhou 213125, China

³ Key Laboratory of Refrigeration and Cryogenic Technology of Zhejiang Province, Institute of Refrigeration and Cryogenics, Zhejiang University, Hangzhou 310027, China

* Correspondence: jianglong@zju.edu.cn

Abstract: Currently, large-volume type IV composite vessel tube trailers garner significant attention and development within the hydrogen energy storage and transportation industry due to their cost-effectiveness and practicality. This study aims to assess the static strength and sealing performance of the boss structure in order to optimize its design. Firstly, a model of the mouth structure of type IV vessels was constructed to analyze the stress distributions in the boss and liner. Subsequently, innovative boss and liner structures were developed based on the primary mouth structure to investigate the impact of geometric dimensions through finite element analysis. This study revealed that changes in geometrical dimensions led to significant alterations in the stresses of the plastic liner in comparison to metallic bosses. Building upon these findings, the structural safety and sealing performance of the boss and liner structure were further validated through finite element analysis. The outcomes of this research can serve as a reference for guiding the structural design of bosses and aiding in the development of hydrogen storage vessels.

Keywords: type IV hydrogen cylinder; boss structure; finite element analysis; sealing structure



Citation: Meng, Z.; Jin, S.; Yu, M.; Mehari, A.; Jiang, L. Analysis of the Boss Structure of Type IV Composite Vessel for a High-Pressure Hydrogen Tube Trailer. *Sustainability* **2024**, *16*, 5098. <https://doi.org/10.3390/su16125098>

Academic Editors: Orazio Barbera, Monica Santamaria and Vincenzo Baglio

Received: 10 May 2024
Revised: 5 June 2024
Accepted: 13 June 2024
Published: 15 June 2024



Copyright: © 2024 by the authors. Licensee MDPI, Basel, Switzerland. This article is an open access article distributed under the terms and conditions of the Creative Commons Attribution (CC BY) license (<https://creativecommons.org/licenses/by/4.0/>).

1. Introduction

At present, nations across the globe are actively pushing for the advancement and utilization of hydrogen power to tackle energy and environmental challenges [1]. One of the most promising areas for hydrogen energy is in the realm of hydrogen fuel cell vehicles, which are significantly anticipated in the market [2]. With near-zero emissions, short refueling time, long range, and high performance, hydrogen fuel cell vehicles are suitable for more than ten types of heavy-duty vehicles (HDVs) that can be used in many scenarios, e.g., logistics and delivery, municipal wastewater disposal, mass transit, public transport, and passenger cars [3–5]. HDVs have consistently been identified as a truly sustainable source of automotive pollutant emissions. Despite commercial vehicles in China representing only 10.9% of total vehicle ownership, they consume 51% of petrol and diesel, with carbon dioxide emissions accounting for 56% and air pollutant emissions for 80% of total vehicle emissions. The Euro 7 regulation, set to take effect in 2025, and the upcoming National 7 standard in China reflect governmental efforts to shift from diesel heavy-duty vehicles (HDVs) to new energy HDVs to decarbonize the transport industry and contribute to upfront the CO₂ emission crisis and temperature rising worldwide [3,6,7].

Nevertheless, hydrogen presents potential dangers including leaks, fires, explosions, erosion from hydrogen, and the potential for cold temperatures, which pose a major challenge to ensuring the safety of hydrogen storage and transportation [8]. High-pressure gaseous hydrogen storage technology provides a temporary solution to advance the development of the hydrogen storage and transportation industry by meeting requirements

such as weight and volume, energy efficiency, durability, and quick refueling times [9–11]. High-pressure gaseous hydrogen storage can be categorized into five groups, including type I to type IV [12]. Metallic cylinders make up type I containers, while type II vessels are metallic cylinders wrapped with carbon fiber composite materials. Vessels of type III and type IV are either lined with metal or polymer and covered with a composite layer on the outside. The composite outer layer is engineered to prevent structural failure due to damage accumulation from fracture or fatigue [13–15], while the liner is designed to withstand high-pressure hydrogen under different thermal and mechanical loads.

In the operational state, high-pressure hydrogen enters or exits all four types of vessels through a longitudinal channel in the opening structure. The opening structure consists of two parts: one is the boss structure, and the other is flow-control devices such as valves, regulators, or nozzles. Figure 1a is a schematic diagram of the connection structure between the polymer liner and the boss structure. The boss structure includes internal thread to ensure firm contact and tight sealing between the hydrogen filling valves [16]. Threads can be incorporated on the outside of the polar boss and the adaptor can be screwed onto the boss structure. There is a sealing gasket between the polymer liner and the bottle seat that prevents hydrogen from escaping. The high-pressure gas inside the cylinder causes the inner liner to adhere firmly to the boss structure. Compared to the boss structure in Figure 1a, the boss structure in Figure 1b is integrated into the bottle seat, eliminating the sealing connection between the bottle seat and the boss structure.

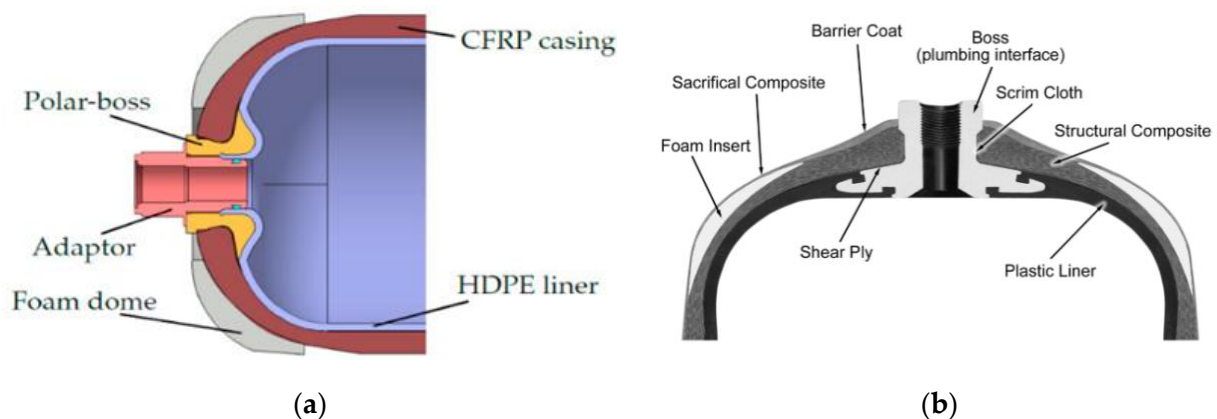


Figure 1. (a) Typical type IV boss structure [17], (b) the boss structure of Hexagon Lincoln for NGV gas vessels [18].

However, fixing the boss structure of the cylinder is always a challenge. In type I and II pressure vessels, hydrogen filling valves are fixed on the metallic body. For type III pressure vessels, the opening of the metallic liner has the same function as the boss structure. However, the use of plastic liner in type IV vessels, such as high-density polyethylene (HDPE) or polyamide (PA), results in hydrogen leakage due to the implementation of composite over boss sections, so how to fix the polymer inner liner to the metal boss structure needs to be considered [19–21]. A polar boss is attached secondarily to the liner and the composite layer. The connection to the flow-control devices is also made via the polar boss, such as shut-off valves and thermally active pressure valves [22]. Due to the ease with which hydrogen can leak out from the plastic liner under high pressure, and the challenge of ensuring the strength of the connection between the metal bottle mouth and the plastic liner, there is a risk of explosion in the fully wrapped carbon fiber reinforced cylinder with a non-metallic liner. Through the investigation of hydrogen safety incidents, it has been determined that piping, fittings, and valves are the components most susceptible to failure, with the boss structure playing a crucial role in these occurrences. One method of connecting to flow-control devices in type IV pressure vessels is to use mechanical threads between the neck and the polar boss fits around the opening of the vessel. Non-

metallic materials to metal adhesive bonding can also be used, although achieving adhesive bonding between non-metallic materials and metal, such as plastic in this case, can be challenging, the substantial pressure within the cylinder can aid in preventing slippage of the liner during pressurization and depressurization. Additionally, both the lower and upper surfaces of the flange section may undergo roughening or other treatments to further prevent sliding.

For years, analytical solutions and numerical analysis in finite element analysis (FEA) [23] were used to investigate the effects of different boss structures. Bouhala et al. [24] delve into the numerical methods, encompassing conventional shell elements, continuum shell elements, three-dimensional solid elements, and specialized homogenization techniques for multilayered composite pressure vessels. The findings suggest that three-dimensional solid elements provide the highest level of accuracy in modeling composite pressure vessels. Continuum shell elements closely follow in terms of accuracy and computational efficiency, as they strike a balance between the two by combining features of both 3D and conventional shell elements. W. William et al. [25] used a metallic insert to connect the dome structure to the valve system in type III vessels and conducted a comparative study between the different insert geometries and locations in the dome. The results showed that an insert extending through the dome geometry increased the resulting stress at the junction between the vessel and the dome. Zhu et al. [26] designed a novel boss structure with sealing grooves, and stop-rotation platforms, which provide close contact between the polymer inner, the boss, and the composite layer under the working pressure. The results showed that the angle of inclination of the stop-rotation platform and the number of sealing grooves in the boss structures can increase fatigue life and sealing performance of the boss structure. Gunyoung Park et al. [27] et al. concentrated on optimizing the contact surface between the boss structure and the dome. They performed an optimal design of the aluminum boss that met the requirements for structural safety verification. However, Gun Young Park's study simplified the boss shape as two cylinders assembled, which is quite different from the actual boss model. Nimdum et al. [28] investigated the influence of the gap, which is induced by debonding between the composite shell and metallic boss during the cooling stage of the curing process on the mechanical behavior of the composite vessel. The results showed that the gap could lead to local bending on the dome area and axial nonlinear behavior response.

The boss structure not only serves to connect to the support frame, but also plays a very important role in ensuring the sealing performance at the mouth of the hydrogen storage vessel [29]. Due to the large difference between the modulus of elasticity and the coefficient of thermal expansion between the metal boss and the plastic, the cyclic pressure load and thermal stresses generated during the repaid filling process will cause cracks in the joint between the boss and the liner, which may lead to gas leakage. If hydrogen escapes, accidents can easily occur due to its inherent properties such as low minimum ignition temperature and wide flammability range. Hence, a study is essential to analyze the sealing performance of the junction structure in order to provide design recommendations for the boss [30]. Tao [31] et al. established a finite element model (FEM) of the bottle mouth structure of type IV pressure vessels using ABAQUS 2020. They investigated how the boss shape and liner thickness impact the deformation and contact stress of the rubber O-ring.

However, these boss structures are mainly used for hydrogen pressure vessels on board, and there is very little research on boss structures used for the vessels on tube trailers [32]. Compared to on-board hydrogen pressure vessels, the bundle gas vessels used in long tube trailers have a larger length-to-diameter ratio. Large-volume hydrogen storage vessels require large port openings for hydrogen charging and discharging, which necessitates special considerations for liner thickness, exotic threads, and complicated composite wrapping patterns around the polar neck. In addition, the vibrations and deflection generated during transportation impose special considerations on the static strength of the boss structural joint [33]. In this paper, the geometric dimensions of the boss structure are considered as a key factor. A model of the vessel mouth is simplified

and the impacts of geometric dimensions on the structure of the boss are studied. On this basis, the influence of the geometric dimensions on the static strength of the boss structure joints is investigated.

2. Finite Element Analysis

2.1. Finite Element Modeling

To solve the problem of possible failure at the joint of the boss structure, numerical analyses based on implicit programs (such as ABAQUS/standard) were performed [34]. ABAQUS is a powerful finite element analysis software with a wide range of element types for structural modeling. For composite hydrogen vessels, ABAQUS has a special module for fast and accurate lay-up design, which is a good method for studying the mechanical behavior of composite vessels.

In ABAQUS, a 2D axisymmetric model could increase the calculation speed, but a 2D model would not accurately model the direction of the lamina fiber, so a 3D FE model is chosen for further simulations [35]. Since the local warp angle and wall thickness in the head region change continuously during the fiber winding process, the head is divided into sixteen segments to accurately simulate the continuous winding process with variable thickness [36,37]. The different ply contours and fiber angle distribution in each fiber section are calculated based on the initial ply thickness and tank radius of each section. The part with the carbon fiber layers is created using the “Merge” function in ABAQUS, and the entire vessel model is also created by the “Merge” function.

In the analysis, the C3D8R cell can be selected to simulate the plastic inner liner and the metallic boss [38]. The cell C3D8R is a 3D cell with 8 nodes that uses reduced integration, offering translational and rotational degrees of freedom in three directions for each node. The advantage of using a reduced-integration cell is that the calculation time for capturing accurate displacement and stress fields is shorter. For the composite fiber layer, the SC8R continuous shell cell is selected for the simulation [39]. This type of cell can simulate the modeling of a solid, but its response is the same as that of a shell cell, so it is used for the simulation of composite laminate structures with higher accuracy and efficiency.

2.2. Grid Independence Verification

To ensure that the FEM calculation can converge, it is necessary to refine the grid. However, increasing the number of cells leads to a higher consumption of computer power and computing time. In this study, the hydrogen storage vessel has a large aspect ratio, so it is necessary to reduce the mesh density at the local positions of the vessel head and the vessel shell. Since the different parts of the hydrogen storage vessel are assembled in the area of the polar boss, the mesh densities need to be refined here. Based on the above requirements, four different mesh numbers were generated, varying between 200,000 and 400,000. The findings can be observed in Table 1, indicating that as the cell count rises, the stress in the fiber direction within the winding layer diminishes, while the Mises peak stress in the inner liner progressively rises. But the difference is not obvious. Considering the computer performance and calculation time, a grid of 320,000 is selected.

Table 1. Comparison of finite element results with different mesh numbers.

Number of Cells	A/204552	B/261136	C/327918	D/393600
Stress in fiber direction/MPa	1372	1343	1329	1313
Stress in the liner/MPa	51.08	52.35	52.10	53.88

2.3. Boundary Condition and Loading

The boundary conditions are determined according to the actual working conditions of the hydrogen storage vessel in the long tube trailer. Cylinders are typically mounted on the traveling mechanism using fasteners to connect them to support plates at both ends of the frame. However, the traditional connection methods may have a potential impact on

the type IV cylinders with a great length-to-diameter ratio in this study, due to the shock and torsion generated in complex road conditions. To address this issue, shock-absorbing cushioning materials like copper, rubber, nylon, and PTFE are often installed at both ends of the support plate. This study simplifies the installation by fully restraining one end and allowing free sliding along the length of the gas cylinder at the other end. While this approach helps mitigate the impact of special road conditions on large-volume cylinders, the free sliding of one end along the cylinder's length may increase deformation values in that direction, deviating from the actual scenario.

In Figure 2, one end of the vessel is defined as the fixed end with zero degrees of freedom. The other end of the vessel is the sliding end with free degrees of freedom. Since the model is axisymmetric, axisymmetric constraints are applied to the cross-section, and the direction of the constraint corresponds to the local coordinate system. The assumed working pressure of this type IV pressure vessel is 52 MPa.

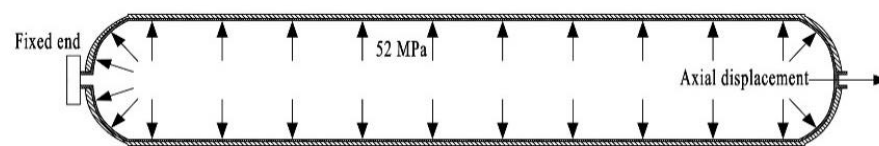


Figure 2. Boundary condition and load of the FEA model.

2.4. Material Properties

The inner liner is made of nylon PA6, and the boss structure is made of aluminum alloy 6061-T6. The specific parameters of the liner and boss structure materials are listed in Table 2.

Table 2. Mechanical properties of aluminum alloy 6061-T6 and nylon PA6.

	Aluminum Boss	Plastic Line
Property	6061-T6	PA6
Elasticity modulus, MPa	70,000	1297
Poisson ratio	0.3	0.38
Tensile strength, MPa	368	
Yield strength, MPa		85
Density, g/cm ³	2.70	1.13

3. Result Discussion

To ensure the connection's safety between the metal boss, liner, and carbon fiber, an exhaustive structural analysis was performed. This comprehensive analysis covered the evaluation of the boss annular flange and transition region, boss-inner liner connection, and the sealing structure of the inner liner through a detailed finite element (FE) model study.

3.1. Boss Annular Flange

After conducting a comparative analysis of boss configurations within the market, it was observed that these structures share certain attributes, and their primary distinction can be attributed to the annular flange segment. To facilitate the analysis, we simplified the boss structure based on the boss planets and took the geometric dimensions of the polar boss part as the factor to explore the influence on the strength of the boss connection. In this section, the radius of the annular flange is selected as a factor influencing the stability.

The schematic diagram of the boss structure with different flange radii is shown in Figure 3, where the flange radius refers to the distance between the axis of the boss structure and the joint of the boss and the liner, and the radii are 60, 70, 80, 85, 90, 95, 100, and 110 mm.

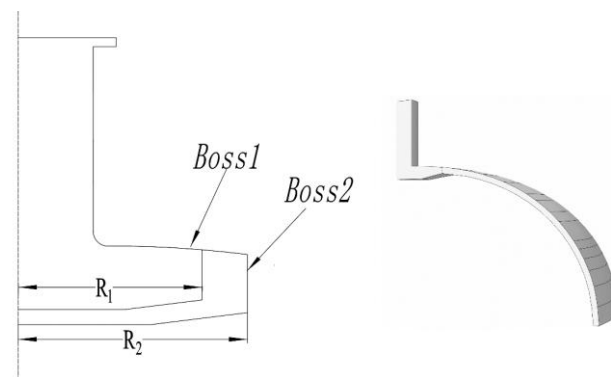


Figure 3. Boss structure with different flange radii.

The Mises peak stress under the working pressure of the liner, the boss structure, and the composite layer on the elliptical head was plotted in Figure 4. Figure 4 shows that the change in the dimensions of the annular flange has a smaller effect on the stress of the boss structure and the maximum Mises stress of the boss at 305 MPa. However, changing the dimensions of the annular flange has a great influence on the maximum Mises stress of the composite layers and the liner. When the flange radius was increased from 60 mm to 110 mm, the peak Mises stress of the liner first decreased and then increased, reaching the minimum stress at 85 mm. The law of change of the fiber was the same as that of the liner, whose peak principal stresses reached the lowest point at a flange radius of 90 mm.

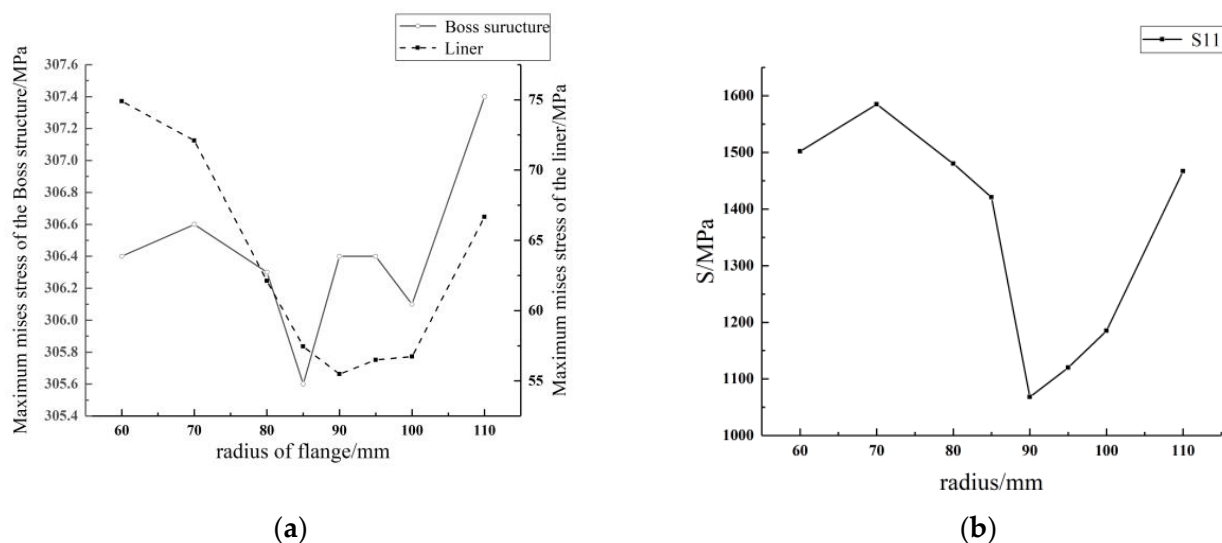


Figure 4. (a) Influence of flange radius on the stress of boss and liner, (b) influence of flange radius on fiber stress of winding layer.

In summary, both the maximum Mises stress of the liner and the maximum principal stress of the fiber are the smallest when the flange radius is between 90 and 100 mm, which means that the boss–liner connection is currently the tightest. Consequently, increasing the flange of the boss structure improves the stability of the connection between the liner and the boss structure.

3.2. Boss Transition Region

The transition area of the boss structure refers to the part of the upper surface of the boss structure that is in direct contact with the fiber winding layer, and which is also the starting point of the fiber winding. Figure 5 shows a schematic representation of the boss structure with three different curved surfaces. Structure A uses rounded corners for a

smooth transition between the neck of the boss and the annular flange, while structures B and C use rounded curves for the transition. The difference between structures B and C is that the curved surface in structure C extends to the edge of the boss flange and the curved surface in structure B extends to the center of the boss flange.

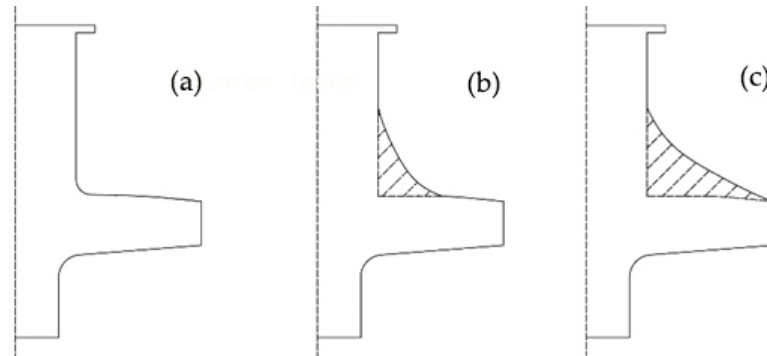


Figure 5. Novel boss structures with different transitional connection sections: (a) structure A, (b) structure B, (c) structure C.

The stress–strain diagrams of the three boss structures under normal working conditions are shown in Figure 6, where the equivalent peak stress and equivalent plastic deformation of boss structure B are the lowest. It can also be seen that the stress in the connection area between the neck part and the annular flange decreases when the transition area is increased, indicating that increasing the transition area can improve the stress state of the neck part. If the stress distribution in the neck area of the boss structure is improved, the strength of the sealing connection between the boss structure and the metal cylinder valve seat can be increased.

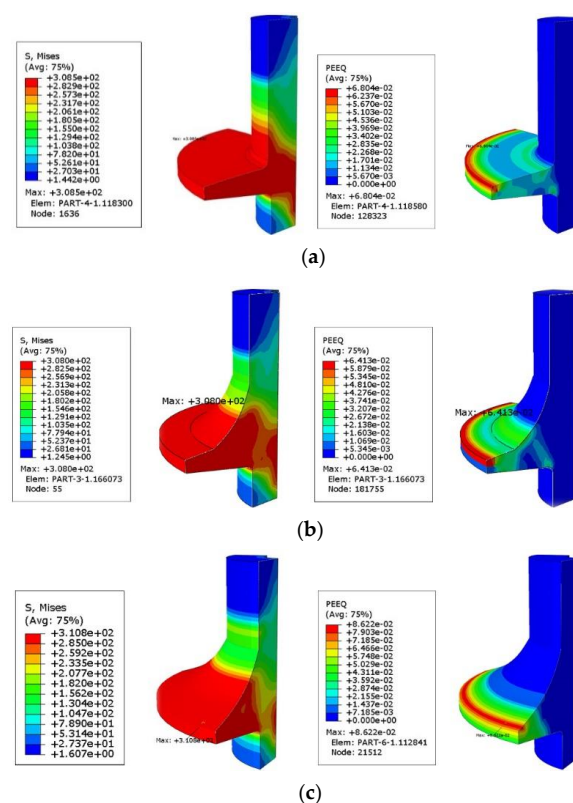


Figure 6. The stress and strain cloud diagram: (a) structure A, (b) structure B, (c) structure C.

In the above diagrams of the stress and strain clouds, the equivalent stress and the plastic strain are always higher at the edge of the annular flange. To reduce the peak values of equivalent stress and plastic strain at the flange edge, five boss structures were placed on the foundations of model B, as the stress is lowest for model B. To improve the stress distribution at the edge of the annular flange, the entire neck area of the boss structure remained the same. Considering that the stresses generated at the edge of the flange are due to the extrusion of the carbon fiber layer, it is possible to modify the curve of the interface between the neck portion and the annular to minimize extrusion, which is shown in Figure 7 as point A. All five boss structures are shown in Figure 7.

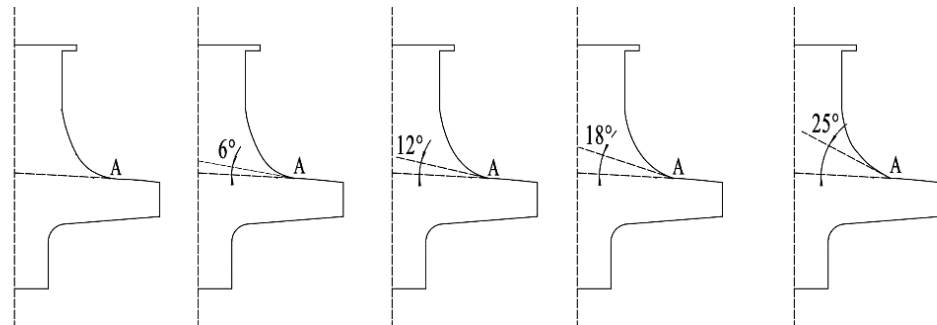


Figure 7. Boss structure with different curvature of contact surface.

The results shown in Figure 8 show that the equivalent peak stress at the edge of the flange first increases and then decreases. Therefore, when it comes to designing the contact surface between the composite layer and the metallic boss, it is better to avoid a boss structure with a tangent angle between 0° and 18° . However, the distance between the results is so small that it can be assumed to have only a minor influence on the boss structure.

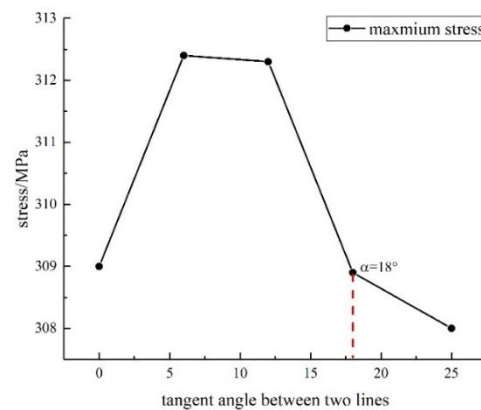


Figure 8. Boss structure stress distribution.

3.3. Boss-Inner Liner Connection Structure Analysis

In the composite vessel, the boss structure is wrapped by carbon fiber and a plastic liner. Compared to the connection located in the boss structure and the carbon fiber, the connection between the plastic liner and the metal boss offers more design flexibility and can have a greater impact on the connection strength.

To investigate the effect of two different plastic liner mouth structures on the strength of the joint, two 3D models were created to calculate the stress of the boss. As can be seen in Figure 9, the liner in structure I has a generally hemispherical end section with a tapered opening aligned with the annular flange of the metallic boss. Typically, the boss has key ways to fit into the opening of the liner or it can be boned to the liner. In structure

II, an elongated double-lip seal structure is provided at the opening of the liner, forming an annular recess between the two lips. The boss structure flange is encapsulated in the annular groove to hold the boss structure securely and firmly. The results are shown in Figure 10.

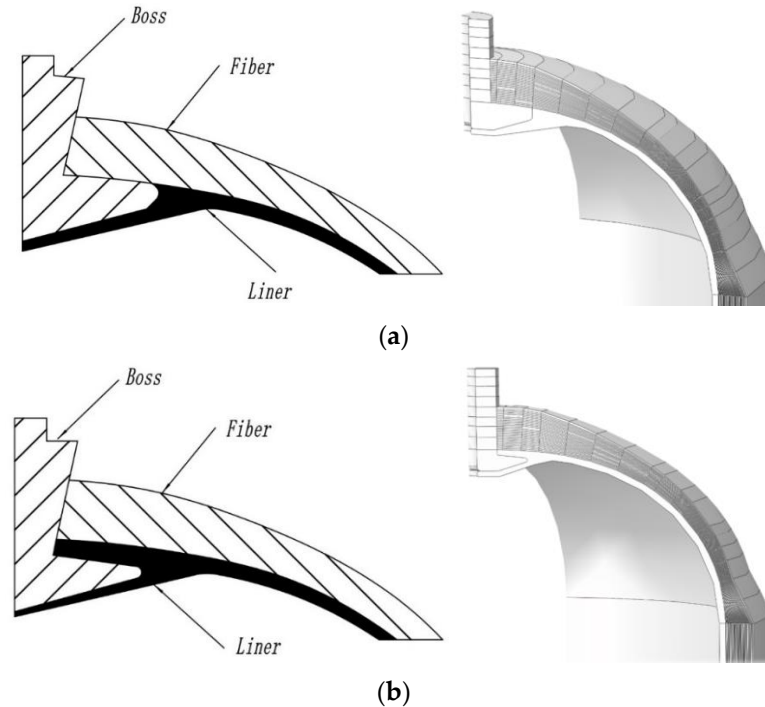


Figure 9. Boss–inner liner connection structure and 3D model: (a) structure I, (b) structure II.

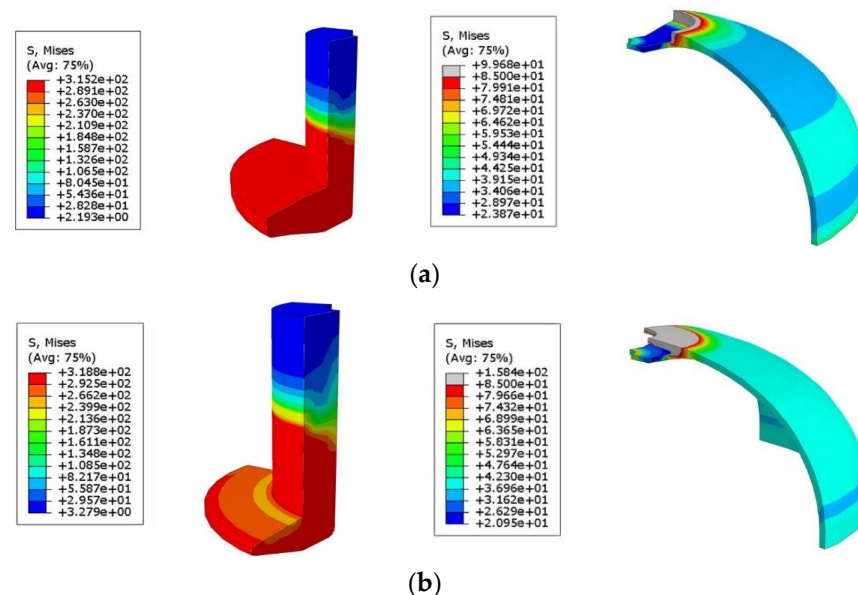


Figure 10. Mises stress in the boss and the liner: (a) structure I, (b) structure II.

To determine the optimal design of the polar boss part, the maximum stress strength criterion serves as a critical constraint, which means the maximum equivalent stresses in the polar boss and liner part must be less than yield strength and tensile strength under the test pressure. At a working pressure of 52 MPa, the maximum compressive stresses of the boss structure occurred in structures A and B at the base of the annular flange, 315.2 MPa,

and 318.8 MPa, respectively, both of which are below the tensile strength of 6061-T6. The Mises peak stress of the plastic liner in the gray area of the stress cloud diagram is greater than the yield strength of the PA6 material of 85 MPa, which does not meet the strength requirements. A Mises stress curve was plotted along the bus line of the liner head, as depicted in Figure 11. The stress is notably high at the opening of the plastic liner, whereas in other regions of the liner, it ranges between 40 and 50 MPa, well below the yield strength of the nylon material. The opening of the plastic liner serves as the junction point between the boss structure, the plastic liner, and the composite layer. The discontinuity of the materials and the structure leads to a phenomenon of stress concentration here, which could lead to the failure of the joint in technical practice.

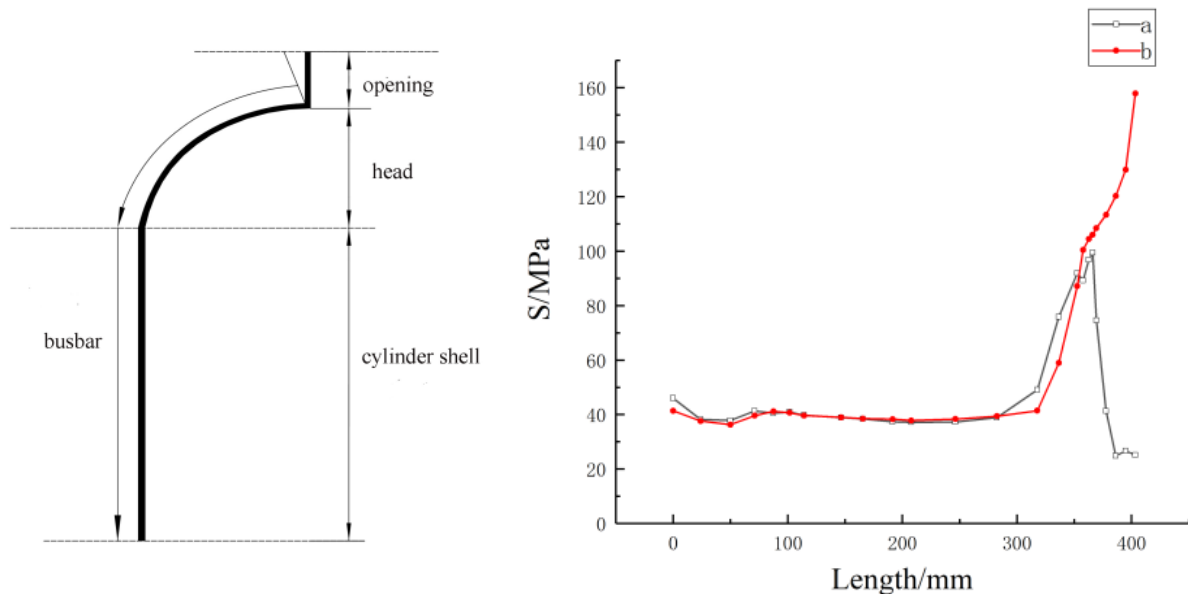


Figure 11. Stress of the liner along the busbar path of the liner.

In structure II, the stress in the opening of the liner increased continuously, with the peak stress far exceeding the yield strength of PA6, indicating that the plastic liner had already failed due to the crushing caused by the high-pressure gas in the container. When the liner is provided with a “double lip” opening, the upper liner is compressed by the metallic boss and the carbon fiber layer. However, the plastic liner is not a pressure-bearing structure, so the enormous pressure can easily cause the liner to fail. Enhancing the torsional strength while minimizing sliding tendencies during cork screwing is achieved by increasing the contact area between the liner and the boss through the unique “double lip” opening structure.

Combining the design features of the connection structure I and II, a connection structure for the liner and the liner using the semi-closed structure is obtained, which is shown in the schematic diagram in Figure 12 with the results of the stress–strain calculations. The figure clearly illustrates that the peak stress experienced by the plastic liner is measured at 81.41 MPa, which is significantly below the yield strength for PA6 material. This indicates that the plastic liner is operating within safe limits under the applied conditions. The peak stress of the boss structure is 311.4 MPa. Compared to structures A and B, the peak stress and the equivalent plastic deformation are significantly lower, so the design requirements are met.

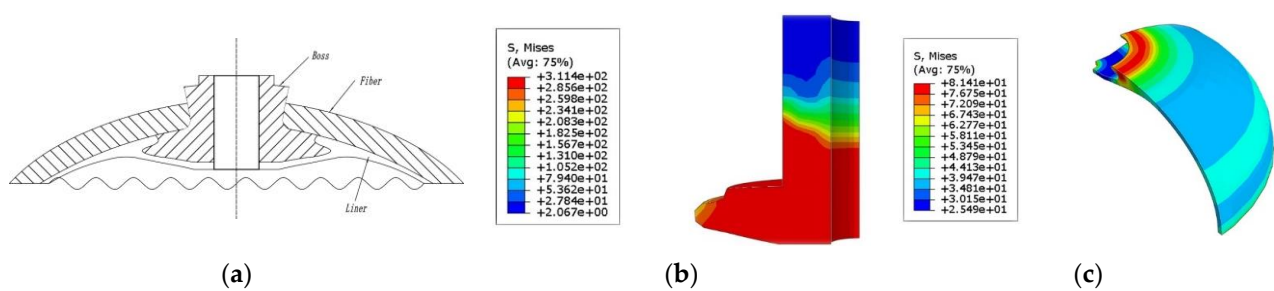


Figure 12. Optimized boss–liner structure and stress: (a) boss–liner structure, (b) stress in the boss, (c) stress in the liner.

3.4. Boss—Research on the Sealing Structure of the Inner Liner

Apart from the connection between the boss and the liner, the sealing structure plays an important role in improving the stiffness and strength of the mouth structure in the composite vessel. In this work, an axisymmetric 2D model (see Figure 13) was created to simulate the sealing structure between the boss and the liner. The stress changes of the O-ring were analyzed under the initial pressure of 0 MPa and the gradual pressure increase. EPDM rubber was chosen as the material for the O-ring, and the strain energy function of the material is described by the Mooney–Rivlin model. The two constants C_1 and C_2 in this function are 0.782 and 0.071, respectively.

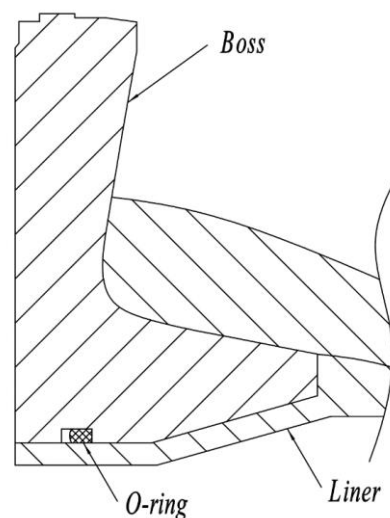


Figure 13. Sealing structure of the type IV vessel.

Secondly, the contact between metal and rubber is considered to be direct contact between a flexible body and a rigid body. The penalty function method is used. The contact between the O-ring and the metal is defined as frictional contact, and the coefficient of friction between the O-ring and the metal is set to 0.1. The coefficient of friction between the O-ring and the plastic is set to 0.04 and the coefficient of friction between the plastic inner liner and the boss is set to 0.02. Finally, the load was applied in two steps. In the first step, a displacement load was applied to the opening to compress the seal. In the second step, pressure was applied to calculate the stress state of the seal structure under actual working conditions.

In the analysis of O-ring sealing performance using finite element methods, von Mises stress and contact stress are key parameters studied under various operating conditions. Von Mises stress is utilized to assess the risk of breakage and fatigue failure in O-rings. Typically, higher von Mises stress levels indicate a higher likelihood of O-ring failure due to potential defects, fractures, or damage. A seal structure is deemed effective in main-

taining good sealing performance when the contact stress exceeds the medium pressure. Figure 14 illustrates that peak contact stresses and mises stresses of the O-ring have a linear relationship with the hydrogen pressure. The black color indicates the von Mises stress, while the red color signifies the contact stress. Additionally, the contact stress of the O-ring surpasses the hydrogen pressure within the vessel at varying pressure levels, indicating that the O-ring may play a sealing role in preventing hydrogen leakage during inflation and pressurization.

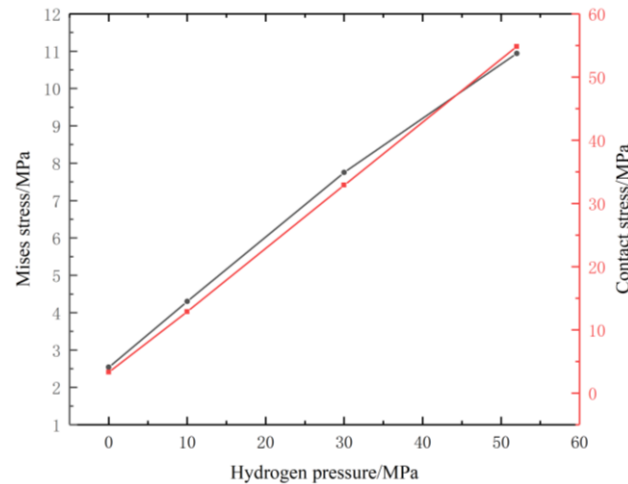


Figure 14. Peak contact stress and mises stress of O-ring in various hydrogen pressures.

In Figure 15, it is shown that the maximum stress of the O-ring is at 0 MPa near the plastic liner. With increasing pressure, the O-ring is pushed towards the space between the metal boss and plastic liner, leading to maximum stress in the extrusion zone. Consequently, failure of the O-ring may happen in this region because of stress concentration, resulting in hydrogen leakage from the gap between the plastic liner and the boss.

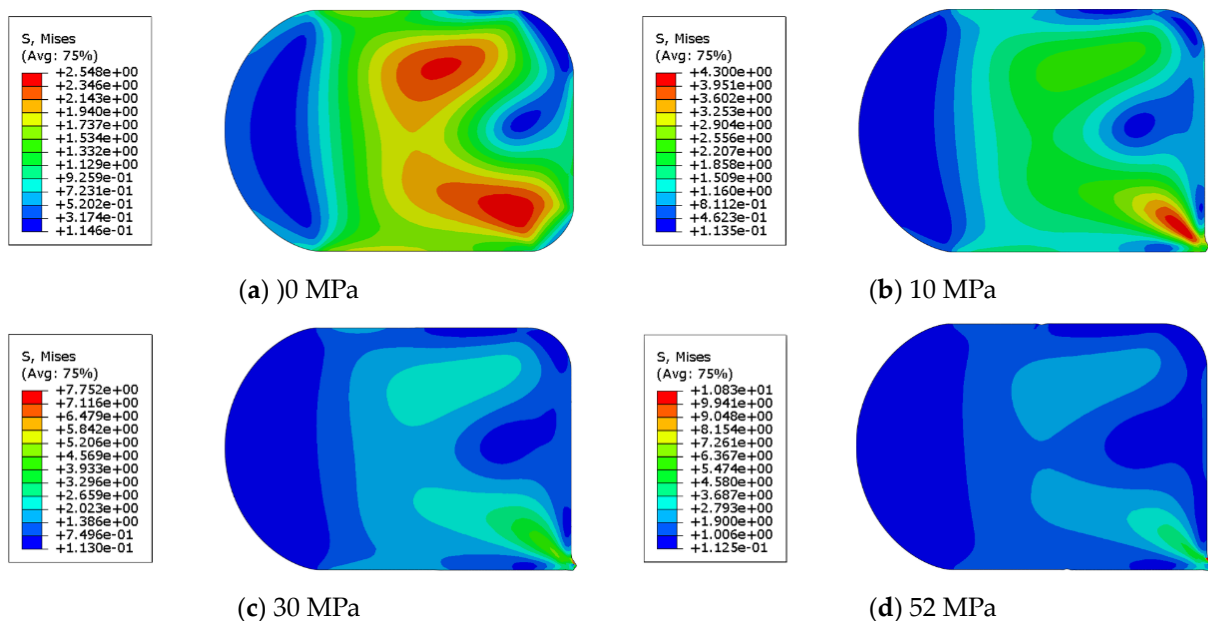


Figure 15. Mises stress contours of rubber rings in various hydrogen pressures.

To improve the sealing performance of the bottle mouth structure, the connection structure between the boss and the inner liner can be improved. The optimization of the

sealing performance of the connection structure focuses on reducing the deformation of the O-ring under high pressure so that it is possible to increase the thickness of the inner liner and use a retaining ring together with the O-ring to avoid the occurrence of extrusion of the O-ring under high pressure.

4. Conclusions

A comparative study of the connection between the fiber, the liner, and the boss was also carried out. In the following, some conclusions are drawn from this work:

(1) As the radius of the annular flange increased, the maximum Mises stresses of the carbon fiber, the metallic boss, and the plastic liner initially decreased and then increased. At a radius of 90–100 mm, the peak Mises stresses of all three components are the lowest.

(2) Changing the shape of the contact surface between the neck and the flange of the boss structure resulted in a reduction of the equivalent peak stress in the boss neck region by less than 2%. In addition, the Mises peak stress at the boss flange edge can be reduced by increasing the discontinuity in the contact area between the metallic boss and the carbon fiber.

(3) When examining the effect of the geometry shape of the boss, the change in shape has a much greater effect on the maximum Mises stress of the liner compared to the boss, which shows that more attention should be paid to the opening structure of the plastic liner when designing the liner–boss joint.

(4) The use of a “double lip” structure in the opening design of the liner may lead to a maximum Mises stress of 110 MPa at the contact surface between the boss and the liner, which exceeds the material yield strength of PA6. Therefore, it is better to use a semi-closed structure for the opening of the liner to meet the strength requirements.

(5) When O-rings are in use, the O-ring is pressed into the gap between the metal boss and the plastic liner by the enormous gas pressure, so that it can fail due to the stress concentration and hydrogen escapes from the gap. Therefore, the sealing performance of the boss–liner structure can be optimized by increasing the thickness of the inner liner and using a retaining ring.

Author Contributions: Conceptualization, Z.M. and S.J.; methodology, Z.M.; software, Z.M.; formal analysis, Z.M.; resources, M.Y.; data curation, Z.M.; writing—original draft preparation, Z.M.; writing—review and editing, A.M. and L.J. All authors have read and agreed to the published version of the manuscript.

Funding: This research was supported by the Key Research and Development Project of Jiangsu Province (BE2022001-5); the Science and Technology Project of State Administration for Market Regulation (2023MK041); the Science and Technology Project of Jiangsu Province Market Supervision Administration (KJ2023001); the Science and Technology Project of Special Equipment Safety Supervision and Inspection Institute of Jiangsu Province (KJ(Y)2023001); and the Jiangsu Provincial Double-Innovation Doctor Program [JSSCBS20230188].

Institutional Review Board Statement: Not applicable.

Informed Consent Statement: Not applicable.

Data Availability Statement: The data presented in this study are available on request from the corresponding author.

Conflicts of Interest: The authors declare no conflicts of interest.

References

1. Reynolds, J.; Ali, D.; Njuguna, J. The State of the Art in Hydrogen Storage. *Green Energy Environ. Technol.* **2023**, accepted.
2. Siddiqui, M.J.; Balguri, P.K.; HariPriya, K.; Rajendran, A.R.; Patil, I.V. Analysis of Type IV Hydrogen Pressure Vessel with S-Glass, Carbon Fiber T700 and Kevlar Composite Materials. *Mater. Today Proc.* **2023**, S2214785323046989. [[CrossRef](#)]
3. Cunanan, C.; Tran, M.-K.; Lee, Y.; Kwok, S.; Leung, V.; Fowler, M. A Review of Heavy-Duty Vehicle Powertrain Technologies: Diesel Engine Vehicles, Battery Electric Vehicles, and Hydrogen Fuel Cell Electric Vehicles. *Clean Technol.* **2021**, *3*, 474–489. [[CrossRef](#)]

4. Li, S.; Djilali, N.; Rosen, M.A.; Crawford, C.; Sui, P. Transition of Heavy-duty Trucks from Diesel to Hydrogen Fuel Cells: Opportunities, Challenges, and Recommendations. *Int. J. Energy Res.* **2022**, *46*, 11718–11729. [[CrossRef](#)]
5. Li, Y. The Economic Feasibility of Green Hydrogen and Fuel Cell Electric Vehicles for Road Transport in China. *Energy Policy* 2022. [[CrossRef](#)]
6. Camacho, M.D.L.N.; Jurburg, D.; Tanco, M. Hydrogen Fuel Cell Heavy-Duty Trucks: Review of Main Research Topics. *Int. J. Hydrogen Energy* **2022**, *47*, 29505–29525. [[CrossRef](#)]
7. Hosseini, S.E. Hydrogen Fuel, a Game Changer for the World’s Energy Scenario. *Int. J. Green Energy* **2024**, *21*, 1366–1382. [[CrossRef](#)]
8. Kang, S.; Kim, H.; Kim, J.; Kim, H.; Jang, J.; Kwak, B.; Choi, K.; Jang, H.-L. Transient Structural Analysis of a Skid Mounted on a Hydrogen Tube Trailer under Shock and Vibration Induced by Road Irregularities. *Appl. Sci.* **2021**, *11*, 3779. [[CrossRef](#)]
9. Roh, H.S.; Hua, T.Q.; Ahluwalia, R.K. Optimization of Carbon Fiber Usage in Type 4 Hydrogen Storage Tanks for Fuel Cell Automobiles. *Int. J. Hydrogen Energy* **2013**, *38*, 12795–12802. [[CrossRef](#)]
10. Sapre, S.; Pareek, K.; Vyas, M. Investigation of Structural Stability of Type IV Compressed Hydrogen Storage Tank during Refueling of Fuel Cell Vehicle. *Energy Storage* **2020**, *2*, e150. [[CrossRef](#)]
11. Rohit, G.; Santosh, M.S.; Kumar, M.N.; Raghavendra, K. Numerical Investigation on Structural Stability and Explicit Performance of High-Pressure Hydrogen Storage Cylinders. *Int. J. Hydrogen Energy* **2023**, *48*, 5565–5575. [[CrossRef](#)]
12. Moradi, R.; Groth, K.M. Hydrogen Storage and Delivery: Review of the State of the Art Technologies and Risk and Reliability Analysis. *Int. J. Hydrogen Energy* **2019**, *44*, 12254–12269. [[CrossRef](#)]
13. Behera, S.; Sahoo, S.K.; Srivastava, L.; Srinivasa Gopal, A.S. Structural Integrity Assessment of Filament Wound Composite Pressure Vessel Using Through Transmission Technique. *Procedia Struct. Integr.* **2019**, *14*, 112–118. [[CrossRef](#)]
14. Rocha, H.; Antunes, P.; Lafont, U.; Nunes, J.P. Processing and Structural Health Monitoring of a Composite Overwrapped Pressure Vessel for Hydrogen Storage. *Struct. Health Monit.* **2023**, 14759217231204242. [[CrossRef](#)]
15. Zhou, W.; Wang, J.; Pan, Z.; Liu, J.; Ma, L.; Zhou, J.; Su, Y. Review on Optimization Design, Failure Analysis and Non-Destructive Testing of Composite Hydrogen Storage Vessel. *Int. J. Hydrogen Energy* **2022**, *47*, 38862–38883. [[CrossRef](#)]
16. Kumar, M. Investigation of Hydrogen Transport Properties through the Liner Material of 70 MPa Type IV Composite Overwrapped Pressure Vessels. *Int. J. Press. Vessel. Pip.* **2024**, *208*, 105150. [[CrossRef](#)]
17. Mahl, M.; Jelich, C.; Baier, H. On the Temperature-Dependent Non-Isosensitive Mechanical Behavior of Polyethylene in a Hydrogen Pressure Vessel. *Procedia Manuf.* **2019**, *30*, 475–482. [[CrossRef](#)]
18. Gheshlaghi, R.M.; Hojjati, M.H.; Daniali, H.R.M. Analysis of Composite Pressure Vessels. In *Fracture of Nano and Engineering Materials and Structures*; Gdoutos, E.E., Ed.; Springer: Dordrecht, The Netherlands, 2006; pp. 335–336. ISBN 978-1-4020-4971-2.
19. Li, X.; Huang, Q.; Liu, Y.; Zhao, B.; Li, J. Review of the Hydrogen Permeation Test of the Polymer Liner Material of Type IV On-Board Hydrogen Storage Cylinders. *Materials* **2023**, *16*, 5366. [[CrossRef](#)]
20. Whisler, D. Damage Tolerance Comparison of Lined Versus Linerless COPVS. Ph.D. Thesis, California State University, Long Beach, CA, USA, 2022.
21. Wang, X.; Tian, M.; Chen, X.; Xie, P.; Yang, J.; Chen, J.; Yang, W. Advances on Materials Design and Manufacture Technology of Plastic Liner of Type IV Hydrogen Storage Vessel. *Int. J. Hydrogen Energy* **2022**, *47*, 8382–8408. [[CrossRef](#)]
22. Patra, S.; Mallisetty, P.K.; Murmu, N.C.; Hirani, H.; Samanta, P. Study on Fracture Evaluation in Hydrogen Environment in 316L Stainless Steel Used in High Pressure Hydrogen Tank. *Mater. Today Proc.* **2022**, *66*, 3723–3728. [[CrossRef](#)]
23. Regassa, Y.; Gari, J.; Lemu, H.G. Composite Overwrapped Pressure Vessel Design Optimization Using Numerical Method. *J. Compos. Sci.* **2022**, *6*, 229. [[CrossRef](#)]
24. Bouhala, L.; Koutsawa, Y.; Karatrantos, A.V.; Bayreuther, C. Design of Type-IV Composite Pressure Vessel Based on Comparative Analysis of Numerical Methods for Modeling Type-III Vessels. *J. Compos. Sci.* **2024**, *8*, 40. [[CrossRef](#)]
25. William, G.W.; Shoukry, S.; Prucz, J.; Evans, T. Finite Element Analysis of Composite Over-Wrapped Pressure Vessels for Hydrogen Storage. *SAE Int. J. Passeng. Cars-Mech. Syst.* **2013**, *6*, 1499–1504. [[CrossRef](#)]
26. Zhu, J.; Li, Y.; Cao, W.; Li, Y.; Gao, Z. Failure Analysis of Novel BOSS Structures for Type IV Hydrogen Storage Vessels. *Energies* **2023**, *16*, 4005. [[CrossRef](#)]
27. Park, G.; Jang, H.; Kim, C. Design of Composite Layer and Liner for Structure Safety of Hydrogen Pressure Vessel (Type 4). *J. Mech. Sci. Technol.* **2021**, *35*, 3507–3517. [[CrossRef](#)]
28. Nimdum, P.; Patamaprohm, B.; Renard, J.; Villalonga, S. Experimental Method and Numerical Simulation Demonstrate Non-Linear Axial Behaviour in Composite Filament Wound Pressure Vessel Due to Thermal Expansion Effect. *Int. J. Hydrogen Energy* **2015**, *40*, 13231–13241. [[CrossRef](#)]
29. Baldwin, D. *Development of High Pressure Hydrogen Storage Tank for Storage and Gaseous Truck Delivery*; DOE-HEXAGON-GO18062 Final Report; Hexagon Lincoln, LLC: Lincoln, NE, USA, 2017; p. 137 3926.
30. Qian, J.; Li, X.; Gao, Z.; Jin, Z. A Numerical Study of Hydrogen Leakage and Diffusion in a Hydrogen Refueling Station. *Int. J. Hydrogen Energy* **2020**, *45*, 14428–14439. [[CrossRef](#)]
31. Tao, J.; Fan, Z.; Xu, P.; Wang, L.; Xue, J. Optimization and Property Analysis of the Sealing Structure of Type IV Cylinder for High-Pressure Hydrogen Storage. In *Proceedings of the Pressure Vessels and Piping Conference*; American Society of Mechanical Engineers: Boston, MA, USA, 2022.

32. Reddi, K.; Elgowainy, A.; Sutherland, E. Hydrogen Refueling Station Compression and Storage Optimization with Tube-Trailer Deliveries. *Int. J. Hydrogen Energy* **2014**, *39*, 19169–19181. [[CrossRef](#)]
33. Deng, G.; Wang, J.; Jiang, Y.; Ji, F.; Feng, J. A Calculation Method for Torques of Large Capacity Cylinders for Tube Trailers. In Proceedings of the Volume 1B: Codes and Standards; American Society of Mechanical Engineers: Boston, MA, USA, 2015; p. 01.
34. Hu, Z.; Chen, M.; Pan, B. Simulation and Burst Validation of 70 MPa Type IV Hydrogen Storage Vessel with Dome Reinforcement. *Int. J. Hydrogen Energy* **2021**, *46*, 23779–23794. [[CrossRef](#)]
35. Johnson, K.; Veenstra, M.J.; Gotthold, D.; Simmons, K.; Alvine, K.; Hobein, B.; Houston, D.; Newhouse, N.; Yeggy, B.; Vaipan, A.; et al. Advancements and Opportunities for On-Board 700 Bar Compressed Hydrogen Tanks in the Progression Towards the Commercialization of Fuel Cell Vehicles. *SAE Int. J. Altern. Powertrains* **2017**, *6*, 201–218. [[CrossRef](#)]
36. Goyal, V.; Rome, J. Analysis Methodology for Assessing Delaminations in Composite Overwrapped Pressure Vessels. In Proceedings of the 53rd AIAA/ASME/ASCE/AHS/ASC Structures, Structural Dynamics and Materials Conference, Honolulu, HI, USA, 23–26 April 2012.
37. Leavitt, M.; Lam, P. *Development of Advanced Manufacturing Technologies for Low Cost Hydrogen Storage Vessels*; DE-FG36-08-GO18055 Final Report; Quantum Fuel Systems Technologies Worldwide, Inc.: Irvine, CA, USA, 2014; p. 1229901.
38. Zhang, Q.; Xu, H.; Jia, X.; Zu, L.; Cheng, S.; Wang, H. Design of a 70 MPa Type IV Hydrogen Storage Vessel Using Accurate Modeling Techniques for Dome Thickness Prediction. *Compos. Struct.* **2020**, *236*, 111915. [[CrossRef](#)]
39. Jiang, Y.; Wei, S.T.; Xu, P. Influences of Filling Process on the Thermal-Mechanical Behavior of Composite Overwrapped Pressure Vessel for Hydrogen. *Int. J. Hydrogen Energy* **2020**, *45*, 23093–23102. [[CrossRef](#)]

Disclaimer/Publisher's Note: The statements, opinions and data contained in all publications are solely those of the individual author(s) and contributor(s) and not of MDPI and/or the editor(s). MDPI and/or the editor(s) disclaim responsibility for any injury to people or property resulting from any ideas, methods, instructions or products referred to in the content.